Nanocrystal growth in alkali halides observed by exciton spectroscopy

M. Haselhoff* and H.-J. Weber
Institut für Physik, Universität Dortmund, D-44221 Dortmund, Germany
(Received 11 February 1998)

We have developed a method to study the growth of CuCl and CuBr nanocrystals in alkali halides by *in situ* absorption spectroscopy. Exciton lines are used as a signature of crystallinity and a broad absorption peak measures the number of Cu^+ ions. The mean radius R and the concentration x_{cr} of nanocrystals are determined simultaneously, which in turn enables the determination of the particle density N of crystals as a function of time. Neither the size-distribution function nor $R(t)$ follow the prediction of the classical growth theory. $x_{cr}(t)$ reveals two different growth mechanisms, one for high and one for low growth temperatures. $N(t)$ demonstrates that the growth of big crystals at the expense of small crystals happens from the beginning of the growth process. This result contradicts the traditional view of Ostwald ripening as a final stage of precipitation and stresses the dynamical character of cluster growth. The experimental data are described by a set of empirical parameters that can be used as a guide for controlled growth of CuCl nanocrystals in NaCl. The smallest nanocrystals detected by exciton spectroscopy consist of 50 unit cells. The kinetic properties of KCl and NaBr crystals doped with CuCl and CuBr are very similar to those observed in NaCl doped with CuCl.
[S0163-1829(98)05732-4]

I. INTRODUCTION

The processes that are responsible for phase separation in the course of a eutectic decomposition are important for the properties of materials, in particular of alloys. They are also important from a more fundamental point of view because grain growth is a rather common phenomenon in nature. Review articles are published from time to time to report the progress mainly of theory.[1–3] For experiments microanalytical tools are needed that are able to detect very small particles (about 1 nm in radius) and to analyze simultaneously their chemical composition. These requirements are fulfilled by only two experimental techniques, direct imaging and small-angle scattering. As usual, both techniques have their merits and their shortcomings. However, none of these techniques has the capability to follow the decomposition reaction continuously from the early stages of nucleation to the final stage of coarsening. We present a technique that does not show this disadvantage without missing the sensitivity to detect clusters with a radius of 1 nm as demonstrated in the present paper. We will analyze not only the chemical composition of the precipitates but also even their state with respect to crystallinity.

Although the phase diagram CuCl-NaCl was determined a long time ago in 1914 (Ref. 4) and although since then the physical properties of this chemical system were studied several times,[5–8] a continuous research work is missing. There exists a simple reason for the only moderate scientific interest in this material. The as-grown crystals are metastable and the relaxation into the stable state needs months and even years. Changes on a long time scale were observed by optical-absorption spectroscopy in the near uv.[5–7] Ueta, Ikezawa, and Nagasaka (1965) (Ref. 8) were the first authors to suggest that microcrystals of CuCl in the NaCl matrix are responsible for the absorption structure near 3 eV. A few years later Fußgänger[9] presented a systematic work in the low doping regime. In this case absorption bands near 5 eV dominate the optical spectrum. In 1988, Itoh *et al.*[10] proved the connection of optical absorption near 3 eV to the size of CuCl crystals embedded in NaCl by small-angle x-ray scattering.

The current interest in CuCl nanocrystals stems from the exciting new effects that originate in the size dependence of quantum phenomena.[11–13] These confinement effects are studied mainly in II-VI semiconductors dispersed in a vitreous matrix. It is possible to prepare CuCl nanocrystals in oxydic glasses, too.[14] However, only in a crystalline matrix can CuCl nanocrystals show a common orientation as recently demonstrated by two-photon absorption experiments.[15] Therefore, in doped alkali halides the anisotropy of the embedded nanocrystals can be observed, but not in doped glasses. Another motivation for the study of CuCl in a crystalline matrix was the investigation of the elastic interaction between nanocrystals and the surrounding lattice.[16] Images of CuCl in NaCl taken with a scanning near-field microscope demonstrated the existence of deformation fields around the embedded nanocrystals.[17] In agreement with this microscopic observation, the increments of the elastic constants in the composite material could be explained by a prestressed NaCl lattice.[16]

In the present work we elucidate the potential of copper-doped alkali halides and of the exciton spectroscopy for studying kinetic processes in the course of phase separation in a eutectic system. In these materials optical-absorption measurements enable the detection of the nucleated copper compounds in the matrix with a high sensitivity, the discrimination of different states of the embedded material, and the *in-situ* observation of growth processes. As these processes are very slow, their time dependence can be recorded with a conventional spectrometer. Furthermore, the eutectic temperatures are rather low and single crystals of the host material are easily prepared. All these properties cause copper-doped alkali halides to model systems for the investigation of mechanisms related to eutectic decomposition.

Recently, we have demonstrated that our idea to study the eutectic decomposition by optical-absorption spectroscopy works in NaCl doped with CuCl.[18] In the present paper we improve the decomposition of the optical spectra, investigate the dependence of growth mechanisms on the growth temperature T_{gr}, and demonstrate that the mean features of the observable phenomena are the same in different material systems.

The experimental techniques are shortly described in Sec. II, and in Sec. III we demonstrate the way to decompose the absorption spectrum into different contributions. This decomposition is the basic step to study kinetic effects by *in-situ* measurements. Section IV presents experimental results obtained in four different samples. In Sec. V the measured time dependence of the mean radius is compared with predictions of the classical growth theory, and the functional dependence of the concentration of crystals on time is analyzed. Some conclusions are discussed in Sec. VI.

II. EXPERIMENT

NaCl and KCl have been grown by the Czochralski technique with a mole fraction of $x=0.01$ CuCl in the melt. Single crystals of NaBr doped with CuBr have been prepared by the Czochralski as well as by the Bridgman technique. We have studied two samples of NaCl doped with CuCl, abbreviated in the following as CuCl:NaCl. The CuCl concentration is $x=0.002$ and $x=0.0008$, respectively. The concentration of CuCl (CuBr) in KCl (NaBr) has not been determined quantitatively. The values of absorption coefficients indicate a rather small copper content. For optical-absorption measurements the crystals are cleaved and the thin slices are mounted into a liquid-nitrogen cryostat that can be used in the temperature range 78–700 K. Each temperature cycle is started above the eutectic temperature T_{eu} in order to create a reproducible state of the sample. It is characterized by a statistical distribution of the copper ions. Then the sample is quenched to the growth temperature T_{gr} at which the absorption between 3 and 5.5 eV is recorded as a function of time. Finally the sample is cooled down to 78 K. At this temperature narrow exciton resonances are observed.

III. DECOMPOSITION OF THE ABSORPTION SPECTRUM

Recently we have demonstrated that the absorption spectrum of copper-doped NaCl can be decomposed into parts stemming from crystalline CuCl and from noncrystalline copper in the matrix.[18] The experiment was performed in a sample with $x=0.002$. In the present paper we consider also samples with a smaller amount of copper. As a consequence of the lower absorption levels, the measurements can be extended to higher photon energies, which reveals a third component in the spectrum. This demands a more elaborate decomposition procedure than applied before.

A. The range of exciton absorption

Due to the concept of excitons, the common movement of holes and electrons requires periodicity. Therefore, the appearance of exciton resonances can be considered as a signature of crystallinity. They are easily identified by the small linewidth at low temperature. Examples of exciton absorption are shown in Figs. 1–3. In particular, Fig. 3 demonstrates the narrowness of exciton peaks and their strong dependence on temperature.

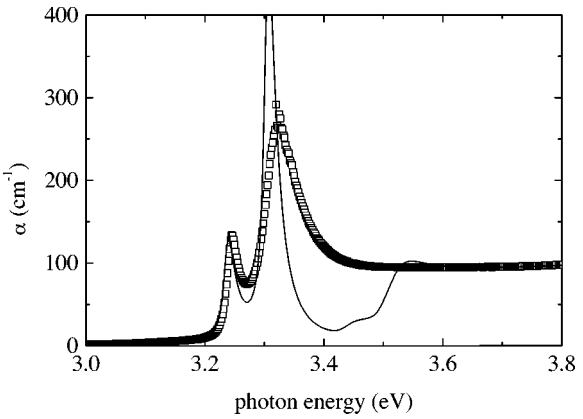

FIG. 1. Absorption spectrum of copper doped NaCl at $T=78$ K (squares). The sharp lines of the Z_3 and the $Z_{1,2}$ excitons indicate the existence of crystalline CuCl in the sample. The solid line represents a theoretical simulation of the absorption spectrum as explained in the text.

Figure 1 shows the Z_3 and the $Z_{1,2}$ exciton of CuCl at 78 K in the NaCl sample with $x=0.002$. Compared with single crystals, the two peaks are slightly shifted towards higher photon energies due to the small size of the absorbing nanocrystals. Efros and Efros[19] developed a theory for spherical nanocrystals with weak confinement. They obtained the confinement energy

$$\Delta E=\frac{\hbar^2}{2M}\frac{\pi^2}{R^2}, \tag{1}$$

where M is the total exciton mass. Equation (1) can be used for nanocrystals with an excitonic Bohr radius smaller than the radius of the nanocrystals. Itoh *et al.*[10] proved by small-

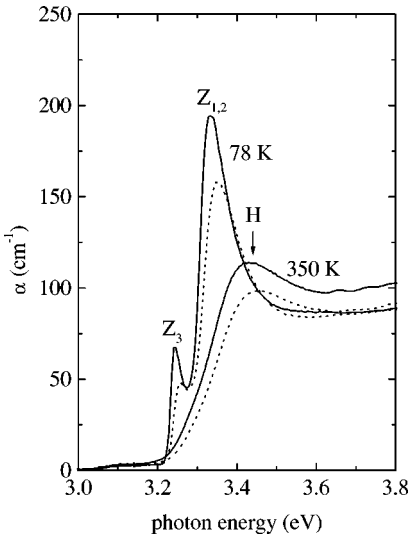

FIG. 2. Absorption of CuCl:NaCl at the growth temperature $T_{gr}=350$ K for two different times. The dotted lines show the absorption after $t=8$ h and the solid lines after $t=20$ h. At $T=350$ K one observes only the broad peak ''*H*,'' whereas at $T=78$ K both exciton lines are resolved.

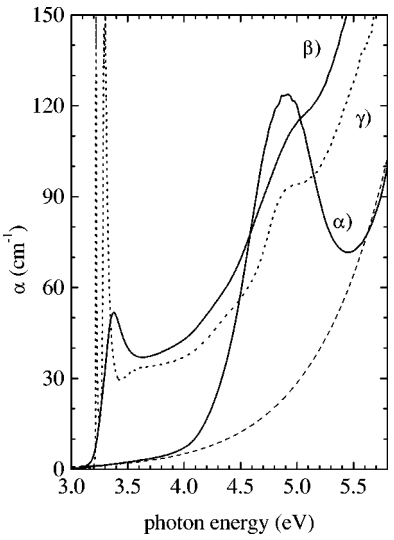

FIG. 3. Decomposition of absorption spectra. Curve (α) reveals the absorption at the initial time of growth at $T_{gr}=400$ K. The spectrum is dominated by a peak at 4.86 eV stemming from ionic copper. For the decomposition we simulated the background by the wing of a Gaussian (dashed line). Curve (β) represents the final absorption spectrum after 23 days at $T_{gr}=400$ K. Curve (γ) is the corresponding absorption at $T=78$ K.

angle x-ray scattering and absorption spectroscopy that Eq. (1) works in CuCl:NaCl with the total exciton mass $M=2.3m_0$ (m_0 is the electron mass) of the Z_3 exciton. Its energy in the bulk is $E_0=3.218$ eV at 78 K.

In the range of excitons the solid line in Fig. 1 is determined in the following way. The total absorption coefficient α_{tot} is calculated as an integral over $\alpha^{\star}(\omega,R)$ of a nanocrystal with radius R weighted with the size distribution function $f(R)$:[19]

$$\alpha_{tot}(\omega)=\int_0^{\infty}\frac{4\pi}{3}R^3\alpha^{\star}(\omega,R)f(R)dR. \qquad (2)$$

In Eq. (2), $\alpha^{\star}(\omega,R)$ is an absorption coefficient per unit volume. The height of the Z_3 exciton is fitted to the experimental data, and the relative height of the two peaks and the energy difference of the peak maxima are taken from the experimental results in single crystals.[20] The peaks are shaped by assuming a size distribution of nanocrystals following the theory of Lifshitz-Slyozov-Wagner (LSW theory) (Refs. 21 and 22) and by using Eq. (1). The experimental peaks in Fig. 1, in particular of the $Z_{1,2}$ exciton, are broader than the calculated ones. Obviously, the real size distribution differs significantly from the LSW theory.

In-situ observation of the growth of nanocrystals includes the analysis of absorption spectra recorded at high temperatures. Figure 2 exhibits experimental curves representing two different states of nanocrystals at two different temperatures. In both cases the spectrum at 78 K was recorded immediately after the measurement of the spectrum at $T_{gr}=350$ K had been finished. At T_{gr} the exciton resonances are much broader than at 78 K. Due to this broadening the two peaks are no longer resolved. In addition, at T_{gr} the maximum value of α, denoted by ''H'' in Fig. 2, is shifted towards higher photon energies. Figure 2 demonstrates that the position of ''H'' is proportional to the positions of Z_3 and $Z_{1,2}$. Therefore, the average radius can be determined also at high temperatures. For each temperature cycle the relation between ''H'' and the peak positions at 78 K was controlled at least one time.

B. The onset of band-gap absorption

Goñi *et al.*[23] have reported a theoretical approach that relates exciton and band-gap absorption in GaAs. Using this theory together with Eq. (2) we have calculated the dependence of α on $\hbar\omega$ for CuCl. The result is the solid line in Fig. 1. The onset of the band-gap absorption associated with the Z_3 and $Z_{1,2}$ excitons appears as steps near 3.45 and 3.55 eV, respectively. The agreement between experimental data and theoretical description above 3.6 eV is striking. Notice that the height of the Z_3 exciton and the mean radius R are the only fit parameters for the whole curve.

The theoretical approach predicts a minimum of α between $Z_{1,2}$ and the band gap. Figure 2 shows the tendency towards such a minimum. Most likely the absorption of extremely small clusters or nanocrystals prevents the evaluation of a pronounced minimum. To avoid any influence of these components on the decompositon procedure, we start the determination of the continuum absorption at 3.7 eV. Its dependence on the photon energy is described by a power series. We have checked that a power series is the appropriate approximation in the single-crystal spectrum up to about 5.2 eV.[24] The area under the absorption curve above the photon energy of 3.7 eV is proportional to the content of CuCl crystals. This is also true for the area below 3.7 eV.

C. Continuum and ionic absorption

Figure 3 shows the spectrum of the NaCl sample with $x=0.0008$. Curve (α) was recorded directly after the sample was quenched from T_{eu} to $T_{gr}=400$ K. The absence of a remarkable absorption at the range of excitons indicates the absence of a crystalline component. A broad peak situated at the photon energy 4.86 eV is the dominant feature in the spectrum. In the past this structure was assigned to sixfold-coordinated Cu^+ ions.[9,25,26] The peak position does not change with temperature. The ionic peak is accompanied by a background that increases strongly with $\hbar\omega$. A similar background is also observed in CuCl:KCl (Fig. 7). The origin of the background is not clear. It is related to a broad peak observed in single crystals of CuCl at 6.8 eV and/or to the absorption of molecular units of CuCl. The dashed line in Fig. 3 represents the wing of a Gaussian peak that describes the background rather well.

Curve (β) in Fig. 3 was recorded after an annealing time of 23 days at $T_{gr}=400$ K. Obviously the onset of exciton and continuum absorption is accompanied by a decrease of the ionic peak. The difference between curve (β) and curve (α) increases from 3.7 eV to 5.5 eV by a factor of 2. A similar increase is observed in the spectrum of CuCl bulk crystals. Curve (β) and curve (γ) differ in the range of exciton absorption, and the ionic peak is less broad at the low temperature, but the dependence of α_{tot} on $\hbar\omega$ in the range of continuum absorption is similar in both curves. The small differences do not permit us to determine the contribution of two different components with high reliability. However, a

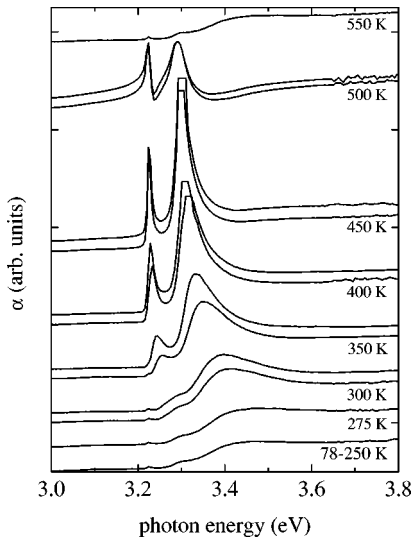

FIG. 4. The temperature dependence of the growth of CuCl nanocrystals in NaCl. The absorption spectra have been recorded at $T=78$ K after annealing at different growth temperatures. The different spectra are shifted along the ordinate. Two ticks are separated by $\Delta\alpha=200\ \mathrm{cm}^{-1}$. The single lines and the first line of each pair have been recorded after $t=8$ h and the second line of each pair after $t=20$ h.

comparison of curve (β) with the dashed line suggests that the background does not change significantly during the growth of nanocrystals. Therefore, in the analysis of data in samples with a low doping level we used the same background for all curves of the same temperature cycle.

IV. OPTICAL SPECTRA AT DIFFERENT GROWTH TEMPERATURES AS A FUNCTION OF TIME

A. CuCl nanocrystals in NaCl

We have heated a NaCl sample with $x=0.002$ up to $T_{eu}=600$ K. As for this concentration the CuCl crystals melt 90 K below T_{eu}, we expect that all clusters are destroyed rather completely. Starting with this state of the sample it is cooled down to the growth temperatures that ranged from 78 K to 550 K. After 8 h annealing at T_{gr} the absorption was measured at 78 K and then the sample was again warmed up to T_{gr}. For $T_{gr}\geqslant 300$ K the measurement at 78 K was repeated after the annealing had been continued for 12 h. The exciton spectra obtained in this way are presented in Fig. 4. The spectra are identical for growth temperatures below 250 K. We attribute the observed absorption to the fact that in the course of cooling between T_{eu} and room temperature some CuCl clusters grow. Two small peaks appear at the positions at which the excitons are expected to appear in the bulk. Their existence can be explained by an unusually high local concentration of CuCl in that sample. We consider this phenomenon to be an artifact of the sample although a similar effect was already reported by Itoh *et al.*[27]

The first indication for the growth of small nanocrystals is obtained for $T_{gr}=275$ K (see Fig. 4). With increasing T_{gr} the exciton peaks shift towards smaller photon energies, which demonstrates an increasing of the average radius R of the nanocrystals. Together with R the amount of nanocrystals increases. The latter trend is reversed for $T_{gr}>450$ K. At

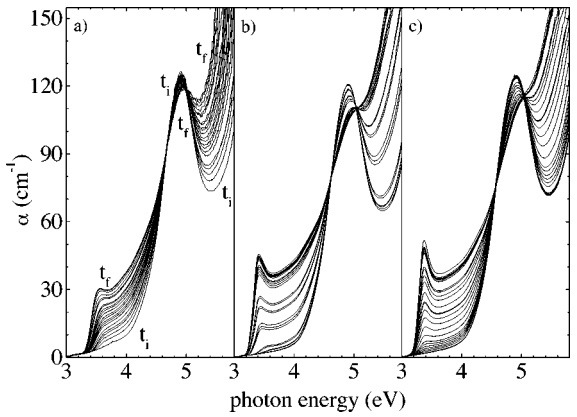

FIG. 5. Absorption spectra of CuCl:NaCl at different times t for three growth temperatures: (a) $T_{gr}=300$ K, (b) $T_{gr}=350$ K, and (c) $T_{gr}=400$ K. The annealing runs start at the initial time t_i and stop at the final time t_f. The steps in time are nonequidistant. The time of a curve can be taken from Figs. 10–12.

$T_{gr}=550$ K no growth at all is observed. The residual absorption is produced during the cooling step as already discussed for $T_{gr}\leqslant 275$ K.

Figure 5 shows absorption spectra of the NaCl sample doped with $x=0.0008$ CuCl at three different growth temperatures. At the initial time t_i the spectra indicate that only single Cu^+ ions exist. For all three growth temperatures the average radius and the crystalline component increase and the ionic component decreases with time. In Fig. 5(a) the final time is $t_f=15$ days and in Fig. 5(c) it is $t_f=23$ days. Roughly spoken, the growth velocity in this sample is slower by a factor 10 than in the sample with $x=0.002$, as can easily be checked by a comparison of Fig. 5 with Fig. 4.

B. CuCl in KCl

The phase diagram CuCl-KCl[4] differs from the phase diagram CuCl-NaCl. It shows the existence of the orthorhombic compound K_2CuCl_3,[28] which renders the preparation of CuCl nanocrystals in KCl more complicated than in NaCl. A few days after crystal growth of the copper-doped KCl crystals, we observed the precipitations shown in Fig. 6. The edges of the quadratic cross sections were parallel to the

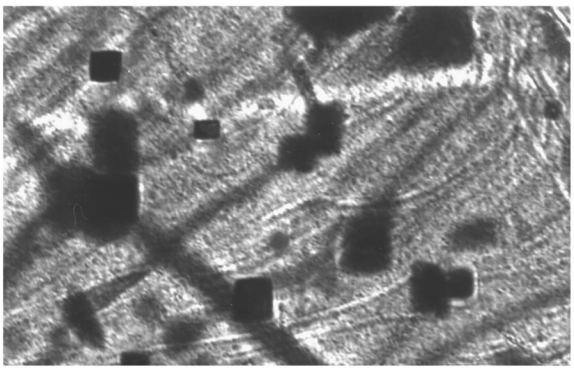

FIG. 6. A typical photograph of freshly grown KCl crystals doped with CuCl observed with an optical microscope. The precipitations have a size of several micrometers. Their edges are parallel to the crystallographic axes of the KCl lattice.

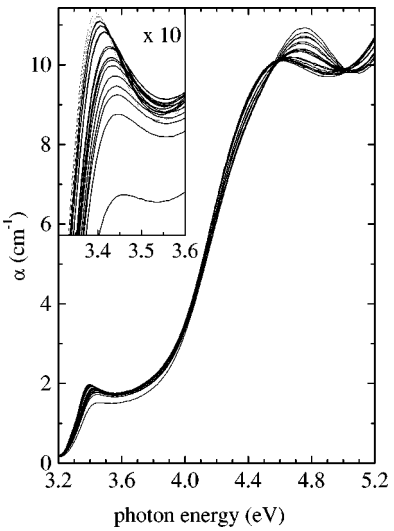

FIG. 7. Absorption spectra of copper-doped potassium chloride at $T_{gr}=330$ K. The excitonic absorption in the inset is tenfold enlarged. The sharpening of the exciton peak by a decrease of α on the high-energy side is accompanied by an increase of the mean radius R demonstrated by the shift of peak position and finally even by a constant value of the ionic absorption. These are direct fingerprints of Ostwald ripening.

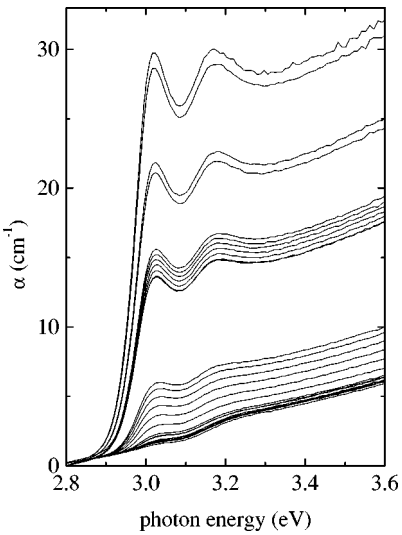

FIG. 8. Growth of CuBr nanocrystals in NaBr at $T_{gr}=400$ K observed with absorption spectroscopy. Due to the larger spin-orbit splitting in CuBr, the $Z_{1,2}$ and the Z_3 excitons are separated even at 400 K. The four groups of curves were recorded with longer interruptions (16 h, 19 h, 60 h). In group one and two the time distance between two curves is 1 h, whereas it is 5 h and 24 h in the two upper groups, respectively. The total time of the experiment is about 8000 min.

crystallographic axes of KCl. We were not able to detect the exciton resonances of the precipitations, even after focusing the beam on one individual precipitation. Two years later the structures on the micrometer scale are absent and now we detect the exciton lines of CuCl.

Figure 7 shows the absorption spectra obtained in a temperature cycle. At the initial time t_i only single Cu^+ ions exist in the sample and with increasing time a crystallization process and a decrease of copper ions is observed. Most interesting is the evaluation of the exciton structure shown in the inset of Fig. 7. After some time, the concentration of Cu^+ remains nearly constant but the maximum of the exciton peak continues to shift to lower photon energies with increasing time. Simultaneously, the absorption coefficient at the high-energy side of the peak decreases. We conclude that the number of small CuCl nanocrystals decreases.

C. CuBr in NaBr

The phase diagram CuBr:NaBr is similar to the phase diagram CuCl:NaCl,[29] but the band structure is different.[24,30] In contrast to CuCl, the energy of the $Z_{1,2}$ exciton is lying below the energy of the Z_3 exciton. The larger spin-orbit splitting in CuBr enables the resolution of both exciton lines even at $T_{gr}=400$ K, as shown in Fig. 8. We have studied the dependence of R and of the content of crystalline CuBr on time at $T_{gr}=300$, 350, 400, and 450 K. For $T_{gr}=300$ K, the velocity of nanocrystal growth is as small as at 275 K in CuCl:NaCl with $x=0.002$ (see Fig. 4). Thus, CuBr:NaBr samples are more stable at room temperature. $\partial R/\partial t$ shows a maximum value at $T_{gr}=450$ K, but the growth rate of the nanocrystalline fraction is maximal at $T_{gr}=400$ K. Figure 8 indicates a time dependence that is similar to the behavior of CuCl:NaCl as discussed quantitatively in Sec. V D. This is easily checked by considering the absorption maximum of the first exciton in Fig. 8 as a function of time.

V. ANALYSIS OF EXPERIMENTAL RESULTS

A. Accuracy of the decompositon procedure

The oscillator strength of the 4.86 eV peak is a measure of the concentration of single Cu^+ ions. Fußgänger calibrated the area under the peak including its dependence on temperature by using samples with a low doping level. Quenching a sample from T_{eu} to $T_{gr}<300$ K conserves the statistical distribution of Cu^+ ions and the total amount of copper can be determined by measuring the peak area. It can be difficult to avoid the nucleation of crystals during the quenching process in samples with a CuCl concentration $x\geqslant 0.002$. We expect the unwanted nucleation, which reduces the experimental accuracy, to depend on the presence of structural defects. The influence of defects on the nucleation process was also concluded from observations in the optical near-field microscope[17] and it is the most natural explanation for the appearance of the bulk excitons in the spectra at 78–250 K and at 550 K of Fig. 4.

In addition to single ions and nanocrystals, there must exist molecular clusters that are too small to show the ideal spectrum of a single crystal and that are too big to contribute to the ionic peak. There exists no clear signature of these clusters. We assume that they contribute to that part of the spectrum we have addressed as background absorption and that is related to the broad structure at 6.8 eV observed in the spectrum of single crystals. It seems to be that this structure is no characteristic signature of crystallinity, which can explain its negligible dependence on annealing. Due to this observation, we assume that at each time of the same cycle the sum of the ionic concentration x_i and of the crystalline concentration x_{cr} is equal to the total concentration x_0. The nomenclature ''background'' is correct in the sense that the assignment to a special state of precipitated CuCl is not possible. In fact, it is an intrinsic component of the CuCl spec-

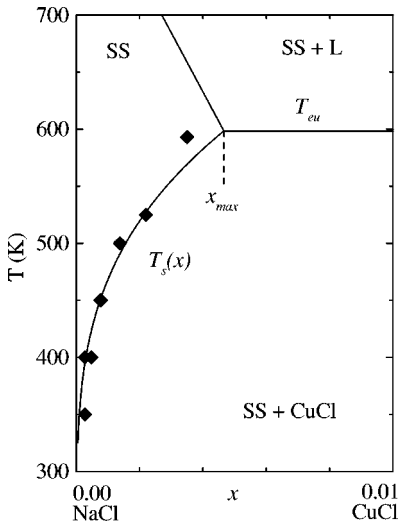

FIG. 9. A section of the eutectic phase diagram CuCl:NaCl at the NaCl rich side. T_{eu} is the eutectic temperature and x is the mole fraction. The subsolidus curve $T_S(x)$ has been determined by a fit of the parameter T_C of Eq. (3).

trum rather than a background. Depending on the treatment of this component, the results vary by 20%.

B. Supersaturation and phase diagrams

From our experimental results the qualitative dependence of the growth of nanocrystals on temperature and concentration is intuitively clear. Diffusion and growth velocity increase with increasing T_{gr}. Growth rates also increase with concentration because the supersaturation Δx increases. However, a quantitative description of the growth processes in terms of temperature and concentration is difficult. One reason is the dependence of Δx on T. $\Delta x(T)$ is determined by the concentration of the Cu^+ ions and by the curve $T_s(x)$ that separates the field of solid solution (SS) from the two-phases field SS-CuCl in the diagram NaCl-CuCl shown in Fig. 9. Our present and our previous results[31] obey the relationship

$$T_s(x) = T_C \frac{2(1-2x)}{\ln[(1-x)/x]} \tag{3}$$

with $T_C = 1580$ K. In order to define supersaturation it is necessary to distinguish different concentrations. x_0, x_i, and x_{cr} have already been defined as the total concentration of CuCl and as the actual concentration of Cu^+ ions and CuCl crystals, respectively. x_s is the final concentration of Cu^+ in the equilibrium state of the sample. The dependence of x_s on T is obtained from Eq. (3).

Our results show that the systems CuCl:KCl and CuBr:NaBr behave in a similar way to CuCl:NaCl. Due to the existence of K_2CuCl_3 in the diagram CuCl-KCl, the growth of CuCl nanocrystals is forbidden. Nevertheless it happens. At the moment we have no satisfying explanation for this phenomenon.

The determination of the miscibility gap in the phase diagram CuBr:NaBr is now in progress. The system can become interesting because the two excitons are easily resolved at high temperatures. Unfortunately, NaBr is strongly hygroscopic. The growth of CuBr in KBr would remove this disadvantage, but the system CuBr:KBr is supposed to contain an additional compound similar to the system CuCl:KCl.

C. Mean radius as a function of time

Traditionally the precipitation processes are considered in three different stages: (i) nucleation of seeds, (ii) growth of seeds to clusters, and (iii) continuing growth of the big clusters at the expense of the small clusters. The latter stage is called
Ostwald ripening. Volmer and co-workers[32] were the first to consider precipitation processes theoretically. Since then the theory was developed continuously and it was used to describe rather different systems.

The theoretical approach predicts the following dependences on time.

(i) The nucleation of seeds is characterized by a constant rate that depends on the diffusion coefficient $D(T)$ and on the supersaturation $\Delta x(T)$:[33,34]

$$J \propto D(T)\Delta x(T)\exp\left(-\frac{\Delta F}{k_B T}\right), \tag{4}$$

where ΔF is the free energy for the formation of seeds and $k_B T$ is the Boltzmann factor. Due to Eq. (4), the number of seeds increases linearly with time. We identified this fingerprint of stage (i) only in one measurement (upper curve in Fig. 12).

(ii) When the seeds grow to clusters, the mean radius increases accordingly to Ref. 35 as

$$R(t) \propto \sqrt{\Delta x(T) D(T) t}. \tag{5}$$

(iii) In the stage of Ostwald-ripening R should increase with time as:[21,22,36]

$$R(t) \propto R_0 + [D(T)t]^{1/3}, \tag{6}$$

where R_0 is the mean radius in the beginning of stage (iii).

The experimental data are tested by use of double-logarithmical plots. The results for CuCl:NaCl with $x = 0.0008$ are presented in Fig. 10. As predicted by Eq. (5), we find straight lines over a rather long period of annealing but their slopes differ from the value $\frac{1}{2}$. Therefore, the most important parameter describing the evaluation of the mean radius is the exponent n in

$$R \propto t^n. \tag{7}$$

The fitted values for n are given in Table I.

As shown in Fig. 10, at long times the exponents become smaller, at least for $T_{\mathrm{gr}} = 400$ K and $T_{\mathrm{gr}} = 350$ K. This decrease may indicate the transition from stage (ii) to stage (iii).

The mean radii at $T_{\mathrm{gr}} = 300$ K are extremely small. As the excitonic structure is well developed in the final spectrum of Fig. 5(a) and as Fig. 10 demonstrates a continuous decrease of R from t_f to t_i, the small value of $R_{\mathrm{min}} = 0.9$ nm for t_i cannot be considered as an artifact due to a wrong determination of R in the first spectrum. R_{min} is equivalent to about 50 unit cells.

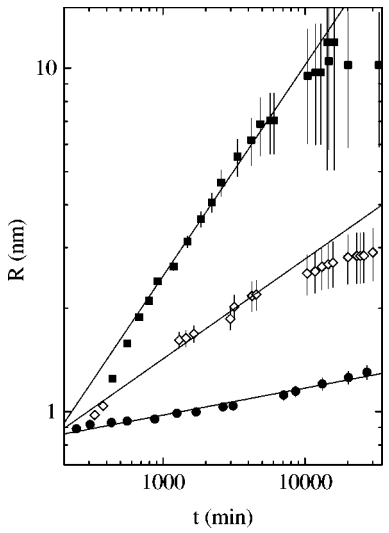

FIG. 10. Increase of the mean particle radius R with time plotted on a double-logarithmic scale for $T_{gr}=400$ K (squares), $T_{gr}=350$ K (diamonds), and $T_{gr}=300$ K (circles). The data are derived from the spectra in Fig. 5.

D. Growth of the crystalline component

In order to describe the increase of the crystalline concentration x_{cr} with time, we start with Fick's second law

$$\frac{\partial x}{\partial t}=\nabla D\nabla x, \tag{8}$$

where D is the diffusion coefficient. Let us assume a homogeneous distribution of Cu^+ produced by heating the sample 50 K or more above $T_s(x)$. Lowering the temperature below $T_s(x)$, the separation into the SS and the crystalline phase CuCl starts by the nucleation of seeds. For the sake of simplicity, we assume that the average distance between two particles $2l$ does not change during the growth process. Using the actual ionic concentration x_i, the supersaturation $\Delta x_i=x_s-x_i$, and the characteristic length l, Eq. (8) is written as

$$\frac{\partial x_i}{\partial t}=\frac{D}{l^2}\Delta x_i. \tag{9}$$

Integrating Eq. (9) and assuming that the total concentration $x_0=x_i+x_{cr}$ is constant during the experiment, we obtain

$$\frac{x_{cr}}{x_i+x_{cr}}=\frac{x_0-x_s}{x_i+x_{cr}}\left[1-\exp\left(-\frac{D}{l^2}t\right)\right]. \tag{10}$$

As shown in Fig. 11, Eq. (10) fits the experimental data recorded at $T_{gr}=400$ K well. The exponential time dependence is also observed at $T_{gr}=350$ K in the same sample and for two growth temperatures in the sample with $x=0.002$. The fit parameters are presented in Table I.

In spite of the small values of R (see Fig. 10), the amount of nanocrystals at $T_{gr}=300$ K is not significantly smaller than at the two higher growth temperatures. In the beginning it is even bigger, as demonstrated in Fig. 11. This result contradicts the fact that diffusion is significantly smaller at the low temperature. Furthermore, the exponential law of growth [Eq. (10)] does not hold. Empirically we find the relationship

$$\frac{x_{cr}}{x_i+x_{cr}}=p+q\ln\frac{t}{t_r}, \tag{11}$$

where p and q are fit parameters and $t_r=1$ min is the reference time. In conclusion, there are several indications that at 300 K the mechanism of nucleation differs from that at higher growth temperatures. It is characterized by a big number of seeds and a logarithmic-growth law for the concentration of nanocrystals $x_{cr}(t)$. A similar result has been obtained by a theoretical model described in Ref. 37. We observe the same phenomenon also in the sample with $x=0.002$ at low growth temperatures. The values of the parameter q in Eq. (11) are presented in Table I.

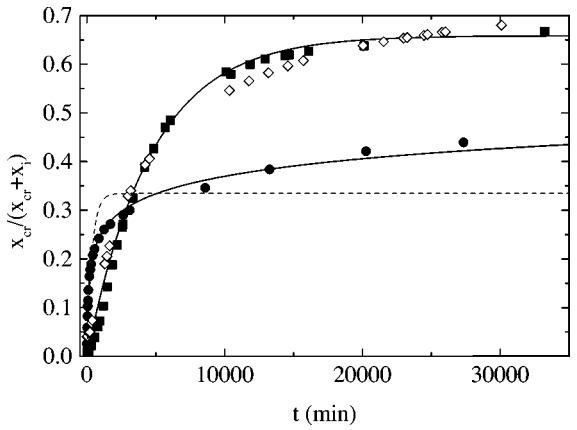

FIG. 11. Increase of the concentration x_{cr} of crystalline CuCl with time. The symbols correspond to those in Fig. 10. For $T_{gr}=350$ and 400 K, $x_{cr}(t)$ is described with Eq. (10) (upper solid line). This function fails for $T_{gr}=300$ K (dashed line). For this temperature Eq. (11) describes the data (solid line).

TABLE I. Parameters for the evolution of R, the crystalline mole fraction x_{cr}, and the particle number N with time at different growth temperatures. The parameters are obtained by best fits of the corresponding equations (7), (10), and (11) to the data. The upper half of the table represents the results for $x=0.002$ and the lower half for $x=0.0008$. The results for the CuCl:KCl sample are given in parentheses. N is given in (10^{16} cm^{-3}) and D/l^2 in (min^{-1}). Δx_s is the abbreviation of $(x_0-x_s)/(x_i+x_{cr})$.

	300 K	350 K	400 K	500 K	(330 K)
n	0.05	0.09	0.13	0.24	
D/l^2			0.03	0.02	
Δx_s			0.71	0.32	
q	0.03	0.02			
N	5.4	3.4	0.7		
n	0.08	0.29	0.57		(0.06)
D/l^2		0.000 17	0.000 21		
Δx_s		0.65	0.66		
q	0.05				(0.02)
N	3.6	0.48	0.01		(0.03)

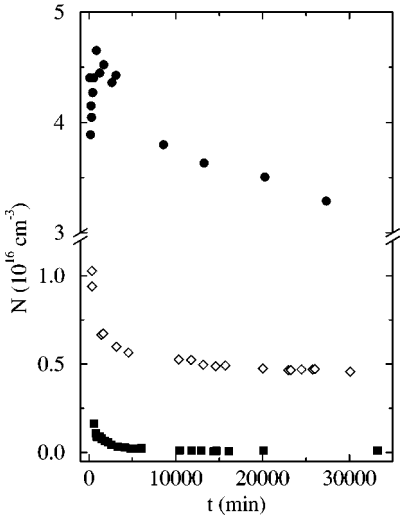

FIG. 12. Particle number N per unit volume of grown nanocrystals as a function of t for different temperatures. Symbols as in Fig. 10.

E. Number of crystals and size distribution

The stage of Ostwald ripening is characterized by the increase of the mean radius and by the constancy of the amount of nanocrystals. Recently we have reported evidence for such a combination in CuCl:NaCl with $x=0.002$ at $T_{gr}=400$ K by comparing $R(T)$ and $x_{cr}(T)$. The change of slopes at $T_{gr}=350$ and 400 K in Fig. 10 probably indicates the transition from stage (ii) to stage (iii), too. The $R(t)$ and $x_{cr}(t)$ curves can only give evidence for the existence of Ostwald ripening. A more decisive quantity is the number of nanocrystals N per unit volume. As Ostwald ripening is characterized by the growth of big clusters at the expense of small clusters, N must decrease with time. Figure 12 exhibits the quantity

$$N=\frac{x_{cr}}{\frac{4}{3}\pi R^3}\frac{V_M(\mathrm{CuCl})}{V_M(\mathrm{NaCl})} \tag{12}$$

for the sample with $x_0=0.0008$ as a function of t. V_M is the molecular volume. At the lowest growth temperature, N increases in the beginning. Apart from this short stage of seed nucleation, N decreases during the whole growth period. This surprising result, which is observed in all samples, contradicts the traditional picture of grain growth in different stages with Ostwald ripening being the final stage.

There is seemingly a contradiction in our analysis of experimental data. x_{cr} is described by an exponential or a logarithmical time law, although the mean radius $R(t)$ follows a potential dependence and $x_{cr}\propto R^3$ seems to be a natural assumption. The contradiction exists because we have neglected any size distribution $f(R)$. To avoid wrong conclusions it is necessary to check its influence, in particular on N. The linewidth Γ of the exciton structures depends on the width Γ_d of the size-distribution function. Here we do not need the exact functional dependence, but only the fact that Γ increases with Γ_d and vice versa. We use the width $\Gamma_{3/4}$ at $\frac{3}{4}$ of the peak maxima at 78 K as a measure of Γ_d. As shown in Fig. 13, $\Gamma_{3/4}$ increases linearly with R^{-2}. The comparison

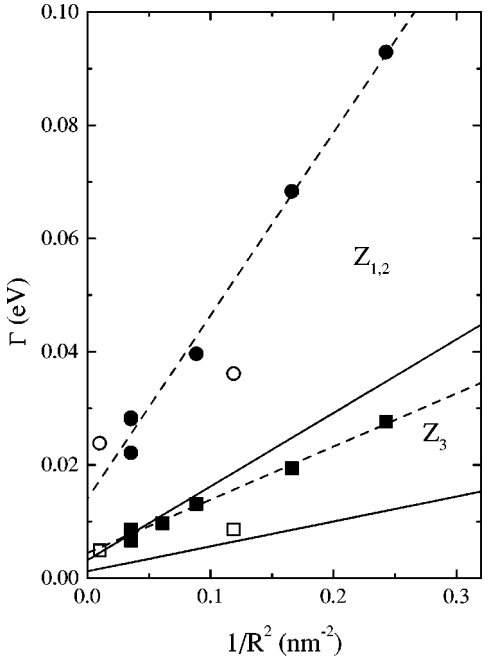

FIG. 13. Width of the exciton lines of CuCl:NaCl at $T=78$ K determined at 3/4 of the peak height. The solid lines represent $\Gamma_{3/4}$ for a simulation of the absorption spectrum by use of Eq. (2) and the Lifshitz-Slyozov distribution function.

with data calculated on the basis of a LSW distribution again demonstrates the bad congruence between experiment and classical theory. Due to Fig. 13, the maximum of Γ_d occurs in the beginning of growth and Figs. 1, 2, 4, and 8 demonstrate that the broadening of the excitons is significantly stronger at high than at low photon energies. The latter effect cannot be explained by the confinement effect alone if a symmetric distribution is assumed. It is necessary to assume that there are more grains with the radius $r<R$ than with $r>R$. Therefore, the negative slopes in Fig. 12 cannot be artifacts introduced by an inadequate management of the size distribution in Eq. (12).

Due to the strong dependence of N on the growth temperature (see Fig. 12) it is a suitable quantity to estimate the efficiency of nucleation. We have included N in Table I by using simply the average of the observed values.

VI. DISCUSSION

A. Experimental progress in growth experiments

Recently, Weaire and Murry[3] reviewed some fundamentals of grain growth and concluded that the congruence of the theory with experiments is very limited. Similar judgments have been mentioned by other authors, too.[1] We believe that the experimental part of the problem can be improved by optical spectroscopy because there are some important advantages over small-angle scattering, which is the leading experimental technique for the study of grain growth. These are as follows.

(i) The richly structured optical spectra provide us with more direct infomation and harder results than the monotonous scans obtained in diffraction experiments.

(ii) The optical measurements discriminate between different states of the precipitations.

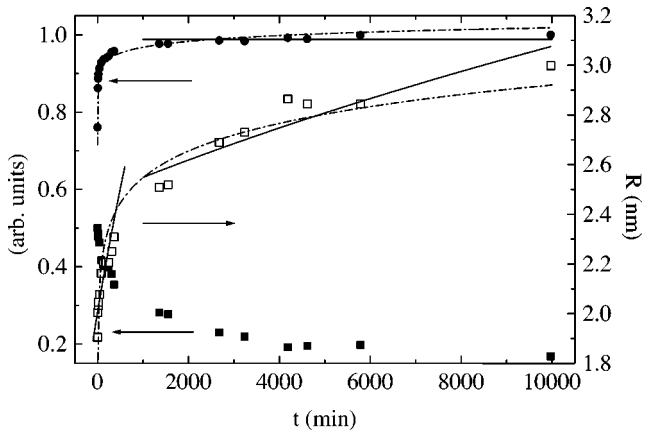

FIG. 14. The growth parameters $R(t)$, $x_{cr}(t)$, and $N(t)$ of CuCl nanocrystals in KCl. The lines represent different kinds of fits as explained in the text.

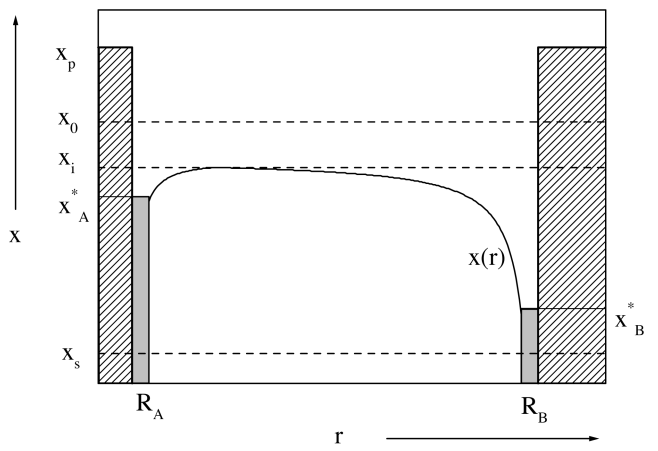

FIG. 15. A schematic plot of the concentration profile $x(r)$ during the precipitation process of CuCl nanocrystals in the NaCl matrix. The hatched areas represent two nanocrystals with the radii R_A and R_B surrounded by a reaction zone (gray area) with the concentrations $x_A^\star$ and $x_B^\star$. The concentration at the surface of a cluster decreases with cluster size, thus $x_A^\star$ lies above $x_B^\star$. The whole content of CuCl is given by x_0. The concentration of CuCl in the clusters is given by $x_p \approx 1$, the actual concentration of Cu^+ ions in the matrix by x_i, and the final ionic concentration by x_s.

(iii) Optical measurements are cheaper and can be performed more easily over a period of several days. Diffraction experiments are usually limited to one day.[38,39]

B. On the comparison of growth experiments with classical growth theory

There are mainly two problems that can be responsible for discrepancies, the simultaneous action of different types of microscopic processes and the complexity of real materials. The first subject is discussed with the assistance of Fig. 14, which shows R, x_{cr}, and N of CuCl:KCl as a function of time. The data are determined from the spectra of Fig. 7. Its inset shows that $\alpha(\omega)$ approaches the shape expected for a LSW distribution. In Fig. 14, $R(t)$ and $x_{cr}(t)$ indicate a sudden change of the slope at $t^\star = 10^3$ min. For $R(t)$, Eq. (5) and Eq. (6) are fitted for $t < t^\star$ and $t > t^\star$, respectively. The solid lines indicate that the classical growth theory seems to work. In accordance with the identification of Ostwald ripening for $t > t^\star$, x_{cr} is nearly constant at this stage. However, the broken lines demonstrate that one potential time law for $R(t)$ and one logarithmical law for $x_{cr}(t)$ fit all experimental data from the beginning to the end nearly perfectly. $N(t)$ demonstrates what really happens. During the whole time of the measurement the seeds and small clusters are dissolved. The velocity of dissolving is extremely different below and above $t^\star$, which causes the sudden changes in the slopes of $R(t)$ and $x_{cr}(t)$ curves.

In our experiments we have observed different phenomena that demonstrate the influence of matrix defects in growth properties. One example is the fingerprint of bulk excitons in the sample CuCl:NaCl with $x = 0.002$ (see Fig. 4). The growth parameters in Table I present a second example. Most striking is the big difference of two orders of magnitude for the parameter D/l^2 in the two CuCl:NaCl samples with $x = 0.002$ and $x = 0.0008$, respectively. The difference in the CuCl concentration is only partly explainable geometrical differences. Recently, we observed in a scanning near-field optical microscope that the growth of big clusters is related to a local assembly of Schottky defects.[17] Such assemblies of defects are able to reduce the diffusion path and the diffusion coefficient drastically and they should influence the primary nucleation of seeds strongly. A nucleation process related to nonideal and disturbed lattices is called heterogenous nucleation.[40] It is manifested in the strong dependence of N on T_{gr} shown in Table I. Obviously, such a strong influence of defects can make a comparison between experimental results and theoretical models useless.

C. The dynamical view of cluster growth

In addition to the accidental influence of defects on the growth properties, there are lawful trends, too. Most striking are three phenomena.

(i) The increase of $\partial R/\partial t$ with T_{gr} as shown by the exponent n in Table I.

(ii) The change of $x_{cr}(t)$ from an exponential time law at high to a logarithmical law at low growth temperatures.

(iii) The continuous decrease of N with t observed in all samples.

Item (iii) is the key result. Obviously there exists a permanent competition between growth and dissolution pointing towards a dynamical cluster growth model. Such a theoretical model was developed by Kampmann, Wagner, and co-workers.[41,42] Unfortunately its application needs numerical methods. Our results suggest that the job could be done by analytical expressions, too.

Figure 15 illustrates a typical situation in the course of phase separation. x_p is the CuCl concentration of the nanocrystal. In our experiments we did not notice any effect indicating a deviation from $x_p = 1$. x_0 is the total and x_s the equilibrium concentration of Cu^+ ions. x_i is the actual concentration of Cu^+ ions in the matrix far away from the precipitated nanocrystals. Figure 15 shows two crystals with different radii. The concentration $x^\star$ in the neighborhood of a nanocrystal depends on its radius. A general relation between cluster size and the concentration $x^\star$ in the reaction zone of a droplet with radius R is given by the Gibbs-Thomson equation[40]

$$x^{\star} = x_s \exp\left(\frac{2\sigma V_M}{R k_B T}\right), \tag{13}$$

where σ is the surface tension. At sufficiently high growth temperatures, $x^{\star} \approx x_s$ (Fig. 15) and the distance between the two nanocrystals A and B is twice the diffusion length. When seeds nucleate their radii will vary. x_i decreases as a consequence of nucleation and continuing growth. As in the beginning the size distribution is broad, it will happen that for some clusters $x^{\star}$ ($x_A^{\star}$ in Fig. 15) exceeds x_i. As a consequence the surface of A is dissolved, which in turn increases $x_A^{\star}$ and thereby the velocity of dissolution, too. With proceeding time the size distribution becomes more narrow and the decrease of $N(t)$ is reduced just as shown by the experimental curves in Figs. 13 and 12. In conclusion, we have the feeling that the cluster dynamical model could be able to describe our experiments even quantitatively, in particular if the preparation of nanocrystals is improved. Such an improvement should be achieveable on the basis of our present results.

ACKNOWLEDGMENTS

We thank K. Reimann for helpful discussions. We gratefully acknowledge financial support by the Deutsche Forschungsgemeinschaft.

*Electronic address: haselhoff@fkp.physik.uni-dortmund.de

[1] R. Wagner and R. Kampmann, in *Phase Transformations in Materials, Materials Science and Technology*, edited by P. Haasen (VCH Publishers Inc., Weinheim, 1990), p. 213.
[2] J. D. Gunton, M. S. Miguel, and P. S. Sahni, in *Phase Transitions and Critical Phenomena*, edited by C. Domb and J. L. Lebowitz (Academic Press, London, 1983), Vol. 8.
[3] D. Weaire and S. McMurry, in *Some Fundamentals of Grain Growth*, Vol. 50 of *Solid State Physics*, edited by H. Ehrenreich and F. Spaepen (Academic Press, San Diego, 1996).
[4] C. Sandonnini, Gazz. Chim. Ital. **44**, 327 (1914) [in E. M. Levin, C. R. Robbins, and H. F. McMurdin, *Phase Diagrams for Ceramists*, 2nd ed. (The American Ceramic Society, Columbus, Ohio, 1969)] .
[5] A. Smakula, Z. Phys. **45**, 1 (1927).
[6] A. MacMahon, Z. Phys. **52**, 336 (1929).
[7] A. Bohun and J. Dolejśi, Mater. Res. Bull. **3**, 463 (1968).
[8] M. Ueta, M. Ikezawa, and S. Nagasaka, J. Phys. Soc. Jpn. **20**, 1724 (1965).
[9] K. Fußgänger, Phys. Status Solidi **34**, 157 (1969).
[10] T. Itoh, Y. Iwabuchi, and M. Kataoka, Phys. Status Solidi B **145**, 567 (1988).
[11] L. Bányai and S. W. Koch, *Semiconductor Quantum Dots*, Vol. 2 of *World Scientific Series on Atomic, Molecular and Optical Physics* (World Scientific, Singapore, 1993).
[12] A. D. Yoffe, Adv. Phys. **42**, 173 (1993).
[13] U. Woggon, *Optical Properties of Semiconductor Quantum Dots*, *Springer Tracts in Modern Physics* Vol. 136 (Springer, Berlin, 1997).
[14] A. I. Ekimov, A. L. Efros, and A. A. Onushchenko, Solid State Commun. **56**, 921 (1985).
[15] D. Fröhlich, M. Haselhoff, K. Reimann, and T. Itoh, Solid State Commun. **94**, 189 (1995).
[16] H.-J. Weber, K. Lüghausen, M. Haselhoff, and H. Siegert, Phys. Status Solidi B **191**, 105 (1995).
[17] A. Diegeler, M. Haselhoff, W. Rammensee, and H. J. Weber, Solid State Commun. **105**, 269 (1988).
[18] M. Haselhoff and H.-J. Weber, Phys. Status Solidi A **164**, 445 (1997).
[19] A. L. Éfros and A. L. Éfros, Fiz. Tekh. Poluprovodn. **16**, 1209 (1982) [Sov. Phys. Semicond. **16**, 772 (1982)].
[20] D. Fröhlich, P. Köhler, W. Niewswand, and E. Mohler, Phys. Status Solidi B **167**, 147 (1991).
[21] I. M. Lifshitz and V. V. Slyozov, J. Phys. Chem. Solids **19**, 35 (1961).
[22] C. Wagner, Z. Elektrochem. **65**, 581 (1961).
[23] A. R. Goñi, A. Cantarero, K. Syassen, and M. Cardona, Phys. Rev. B **41**, 10 111 (1990).
[24] M. Cardona, Phys. Rev. **129**, 69 (1963).
[25] W. Dultz, Phys. Status Solidi **34**, 95 (1969).
[26] S. Payne, A. Goldberg, and D. McClure, J. Chem. Phys. **81**, 1529 (1984).
[27] T. Itoh *et al.*, J. Lumin. **60&61**, 396 (1994).
[28] C. Brink and C. MacGillavry, Acta Crystallogr. **2**, 158 (1949).
[29] R. M. Biefeld, Mater. Res. Bull. **10**, 1151 (1975).
[30] A. Goldmann, Phys. Status Solidi B **81**, 9 (1977).
[31] M. Haselhoff and H.-J. Weber, Mater. Res. Bull. **30**, 607 (1995).
[32] M. Volmer and A. Weber, Z. Phys. Chem., Stoechiom. Verwandtschaftsl. **119**, 277 (1926).
[33] R. Becker and W. Döring, Ann. Phys. (Leipzig) **24**, 719 (1935).
[34] R. Becker, Ann. Phys. (Leipzig) **32**, 128 (1938).
[35] H. B. Aaron, D. Fainstein, and G. R. Kotler, J. Appl. Phys. **41**, 4404 (1970).
[36] D. A. Huse, Phys. Rev. B **34**, 7845 (1986).
[37] G. F. Mazenko, O. T. Valls, and F. C. Zhang, Phys. Rev. B **32**, 5807 (1985).
[38] P. Staron, M. Haese-Seiller, R. Kampmann, and R. Wagner, Physica B **234-236**, 989 (1997).
[39] G. B. Stephenson, W. K. Warburton, W. Haller, and A. Bienenstock, Phys. Rev. B **43**, 13 417 (1991).
[40] W. J. Dunning and E. Hornbogen, *Nucleation*, edited by A. C. Zettlemoyer (Marcel Dekker, New York, 1969).
[41] R. Kampmann, T. Ebel, M. Haese, and R. Wagner, Phys. Status Solidi B **172**, 295 (1992).
[42] R. Kampmann and R. Wagner, in *Decomposition of Alloys: The Early Stages*, 2nd Acta-Scripta Metallurgica Conference, edited by P. Haasen, V. Gerold, R. Wagner, and M. F. Ashby (Pergamon Press, Oxford, 1983), p. 91.